ATLAS Electroweak results

Giuseppe Salamanna[*][†]

Nikhef

E-mail: salaman@nikhef.nl

We present the first results on electroweak physics obtained by the ATLAS experiment at the CERN Large Hadron Collider (LHC), using $p - p$ collisions at a centre-of-mass energy of 7 TeV. The observation of the W and Z electroweak bosons in leptonic decays and the first measurements of their production cross-section at $\sqrt{s} = 7$ TeV represent one of the most important benchmarks of the first stage of data-taking at the LHC and provide a first confirmation of the Standard Model (SM) predictions. Furthermore they are an important candle to understand and calibrate the ATLAS detector with early data. We describe the experimental techniques, issues and the measurement results, together with a comparison with SM expectations, using up to 225 nb^{-1} of integrated luminosity. A first look at the W and Z production as a function of the number of accompanying jets is also provided. Finally, a first search for $t\bar{t}$ production and a comparison of the identified candidates with the expected kinematic distributions from simulation is described.

---

[*]Speaker.

[†]on behalf of the ATLAS Collaboration.

1. Introduction

With the first pp collisions of the Large Hadron Collider (LHC) at CERN in Geneva at the centre-of-mass energy of 7 TeV at the beginning of 2010, a new era of exploration in particle physics has started. The new energy range explored will allow us to probe the validity of models beyond the Standard Model (SM) of particle physics and possibly discover new particles.

Before the discovery phase is reached, though, the LHC experiments have to undergo a phase of comprehension and calibration of the detector response and understanding of the SM processes and their rates with the early LHC data. The SM electroweak bosons, the *W* and *Z*, are among the first particles expected to be observed, given their predicted production cross-sections. Given our good knowledge of their properties [1] from previous experiments, they constitute an important candle by which we can check the response of the detectors. Furthermore, the measurement of their production rate is among the first tests of validity of the SM at $\sqrt{s} = 7$ TeV. In particular, their decays into leptons (electrons and muons) provide a clean enough signature to identify their production in an inclusive sample with an arbitrary number of jets present. The ATLAS experiment [2] at the LHC has started its electroweak physics program by performing a measurement of the *W* and *Z* production cross-section in the $\ell\nu$ and $\ell\ell$ ($\ell = e, \mu$) channels with 17 and 225 nb^{-1} of integrated luminosity respectively. These are just the first of a series of measurements of SM processes involving *W* and *Z*, as a function of kinematic properties and accompanying jet multiplicity, which necessitate a higher statistics data sample. In addition, these processes are among the most important backgrounds to the production of a pair of *top* quarks, $t\bar{t}$ in the semi- and di-leptonic channels. The top quark is the next particle that ATLAS needs to observe on the road towards new physics, inducing signatures in the detector similar, for example, to those from decays of supersymmetric particles.

2. The ATLAS Detector

The ATLAS detector is a general purpose detector with a cylindrical symmetry, using classical detection techniques to reconstruct charged and neutral particles and measure their momentum and energy. The inner-most part is the Inner Detector (ID) system, providing tracking information for charged particles: the silicon tracking detectors, pixel and silicon microstrip, in the pseudorapidity range $|\eta| < 2.5$, provide a fine granularity around the vertex region. The Transition Radiation Tracker (TRT), which surrounds the silicon detectors, adds further track points up to $|\eta| = 2.0$. ATLAS identifies electrons using the transition radiation in the TRT straw tubes and associating the electron track information with the energy release in the EM calorimetry. This system covers the pseudorapidity range $|\eta| < 4.9$. It is based on liquid argon as active media. The EM calorimeter, consisting of lead absorbers and liquid argon as the active material, is divided into several layers, which ensure radial containment of the EM shower shape from $e^{\pm}$ and photons; and rejection of hadronic showers. In the region $|\eta| < 1.8$, a presampler detector is used to correct for the energy lost by electrons, positrons, and photons before they reach the calorimeter.

The hadronic tile calorimeter is placed directly outside the EM calorimeter envelope and covers a pseudorapidity region up to $|\eta| < 3.2$, allowing us to measure the energy of hadronic interactions. Muon detection is ensured by a three-stage muon spectrometer (MS) based on the magnetic de-

flection of the muon trajectory in the large superconducting aircore toroid magnets generating a magnetic field in the pseudorapidity range $|\eta| < 2.7$. The central region ($|\eta| < 1.0$) and the forward regions ($1.0 < |\eta| < 2.5$) are instrumented with separate trigger and high-precision tracking chambers. The first-level (L1) trigger system uses a subset of the total detector information to make a decision on whether or not to record each event, reducing the data rate to a design value of approximately 75 kHz. The subsequent two levels, collectively known as the high-level trigger, are the Level-2 (L2) trigger and the event filter. They provide the reduction to a final data-taking rate designed to be approximately 200 Hz.

3. Monte Carlo simulation samples

We show several comparisons to expectations based on Monte Carlo simulations. For the *W* and *Z* boson studies, the signal and background samples used in this note were generated at $\sqrt{s} = 7$ TeV with PYTHIA [3] using MRSTLO* [4] parton distribution functions (PDF). For the $t\bar{t}$ studies, we use MC@NLO [5] v3.41, with PDF set CTEQ66 [6], assuming a top mass of 172.5 GeV and normalizing the $t\bar{t}$ cross-section to the prediction of [7], which is consistent with other Next-to-Leading-Order (NLO) calculations. More details can be found in [8]. In all cases, generated samples are then simulated using GEANT4 [9] and fully reconstructed.

4. Object reconstruction

4.1 Leptons

Lepton (e, μ) reconstruction is a crucial of the analysis presented here, as only leptonic *W* and *Z* boson decays are considered to extract the production cross section; also for $t\bar{t}$ only the single- and di-lepton channels are considered.

4.1.1 Electrons

The electron reconstruction in ATLAS is based on the combination of a track in the Inner Detector and an energy deposit in the EM calorimeter. The transverse energy of the electron candidate is obtained from the corresponding calorimeter clusters, while its identification relies on a series of selections on both the calorimeter and ID measurements; and the matching of the two. Three reference sets of selections (*Loose, Medium and Tight*) have been chosen, providing progressively stronger jet rejection at the expense of some identification efficiency loss: *Loose*: simply an energy release in the second layer of the EM calorimeter and a matching ID track are required to be present; *Medium*: additional requests on the energy deposit patterns in the first layer of the EM calorimeter, track quality variables and the matching of the two are applied, for a more effective rejection against hadrons; *Tight*: this selection poses tighter track cuts and rejects electrons and positrons from γ conversions.

4.1.2 Muons

Muons are identified as a result of the combination of different sub-detector technologies which provide complementary approaches and cover pseudorapidities up to 2.7. The identification of the kind of muons used for the results presented here starts as stand-alone reconstruction in

the MS, specifically from combining straight line track segments and hits in the precision chambers in three dimensions, accounting for the magnetic field. Then the fitted standalone MS track is combined with an Inner Detector track using a χ^2-test, defined from the difference between the respective track parameters weighted by their combined covariance matrices. The muon reconstruction efficiency, measured directly on data, is $> 93\%$ [10].

4.2 Missing transverse energy

The energy missing in the plane transverse to the beam line (E_T^{miss}) is a valuable tool to select W boson leptonic decays and reject secondary leptons from the large wealth of QCD processes, due to the presence of the neutrino. It is based on both calorimeter and muon information. It relies on a cell-based algorithm summing up the electromagnetic-scale energy deposits of calorimeter cells inside three-dimensional topological clusters. A correction is then applied to the clusters to account for the different response to hadrons than to electrons or photons, dead material losses and out-of-cluster energy losses. The calorimetric part is then summed with the p_T of muons and the muon energy loss in the calorimeters is removed from the calorimeter term. Figure 1 shows the E_T^{miss} distribution in data and simulation for the electron and muon channels
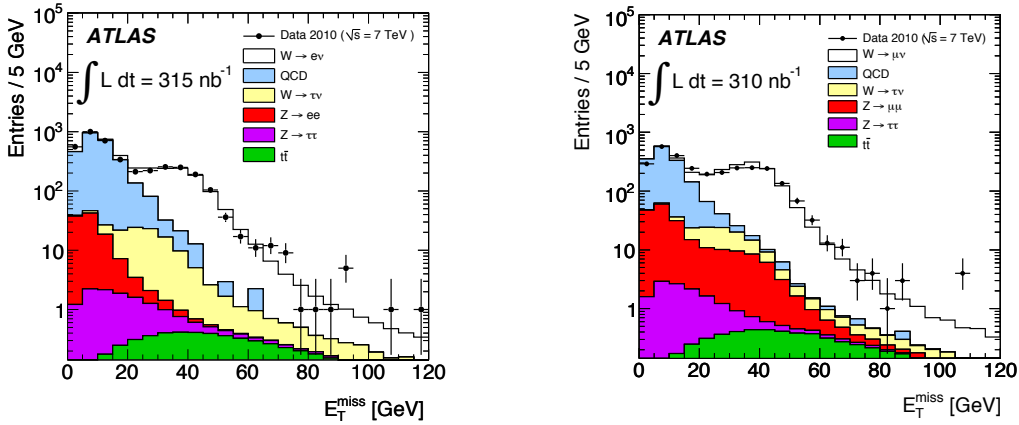

Figure 1: E_T^{miss} of electron (left) and muon (right) candidates after preselection for data and Monte Carlo candidates broken down into the various signal and background components. The integrated luminosity is 310 nb^{-1}, corresponding to a larger data set than the one used for the measurement.

5. W and Z boson production cross-section measurements

In this section we present the analysis and results of the W and Z boson cross-section measurements, performed with 17 nb^{-1} and 225 nb^{-1} of integrated luminosity respectively. The event selections are spelt out and the resulting distributions for the leptons and E_T^{miss}, including their agreement with simulation, are shown. These represent important comparisons in the process of understanding and calibrating the detector response with early data. The signal acceptance, estimation of backgrounds and final measured production cross-sections for the gauge bosons are presented.

5.1 *W boson analysis*

5.1.1 Event selection

In both the electron and muon channel, the main background to the $W \rightarrow \ell \nu_\ell$ decays are represented by decays of (mainly) Heavy Flavour (HF) quarks within jets originated in QCD processes, in which "fake" leptons are created, as opposed to the prompt leptons from electroweak decays. Despite the absence of a neutrino (thus sporting on average a low E_T^{miss}), these generic QCD processes have production cross-sections up to 10^5 times as big as the W boson one; and therefore occur in rates comparable with the signal. An additional sizeable background is the decay of (mainly) $W \rightarrow \tau \nu_\tau \rightarrow (\ell \nu_\ell) \nu_\tau$.

In order to suppress the backgrounds, enhancing the signal-to-background ratio, the following event and object-based selections are applied in the *electron* channel:

- the event is selected by the ATLAS Level-1 trigger requiring $|\eta(\text{calorimetric object})| < 2.5$ and $E_T > 5$ GeV;

- exactly one *Tight* electron reconstructed offline, with an energy in the transverse plane $E_T > 20$ GeV;

and *muon* channel

- the event is selected by the ATLAS Level-1 trigger requiring $|\eta(\text{muon object})| < 2.4$ and $E_T > 6$ GeV;

- exactly one *Combined* muon reconstructed offline, with a momentum in the transverse plane $p_T > 20$ GeV;

- the sum of the p_T of ID tracks closer than $\Delta R = 0.4$ to the muon, normalized to the muon p_T should be less than 0.2, as an isolation criterion;

In both cases, the missing energy in the transverse plane is required to be larger than 25 GeV and the reconstructed W boson mass in the transverse plane, defined as

$$M_T(W) = \sqrt{2(p_T^\ell)(E_T^{miss})[1 - cos(\phi^\ell - \phi^{E_T^{miss}})]} \tag{5.1}$$

should be larger than 40 GeV. Figure 2 illustrates the level of agreement between data and Monte Carlo simulation in terms of the kinematics of the leptons passing the above selections. The simulated distributions match real data already at a remarkable level, even at this initial stage of data taking. In Figure **??** and 4 the distributions of the reconstructed W p_T and $M_T(W)$ for signal and backgrounds are shown, before and after the $E_T^{miss} > 25$ GeV cut. It can be seen that the missing transverse energy requirement rejects a considerable part of the QCD background, as expected; and that the $W \rightarrow \tau \nu_\tau$ becomes predominant, but still approximately two orders of magnitude less large than signal. The effect of the various individual selections on the number of events is quantified [11]. After all the above requirements, 46 (72) events are selected in the electron (muon) channel at 17 nb^{-1}. The difference is largely due to the lepton identification efficiency between electrons and muons, given a similar level of rejection of "fake" leptons from QCD.
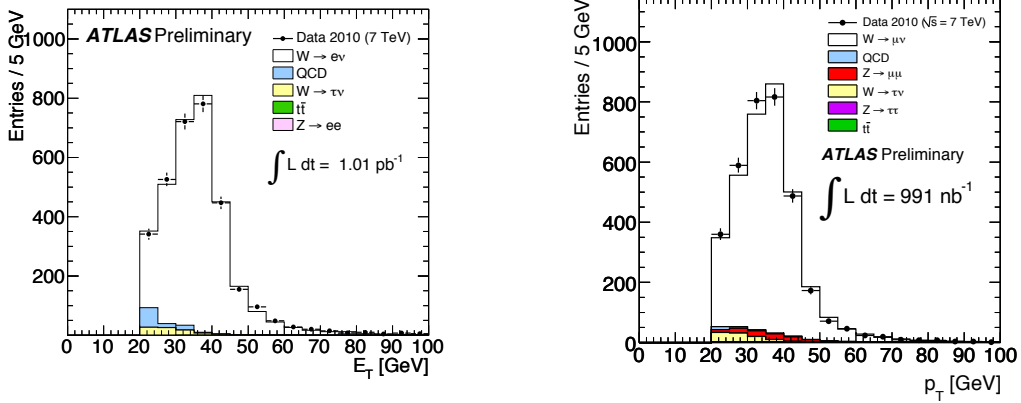
Figure 2: Electron cluster E_T (left) and muon p_T (right) of the W candidates after final selection. The integrated luminosity is $\approx$ 1 pb^{-1}, corresponding to a larger data set than the one used for the measurement.
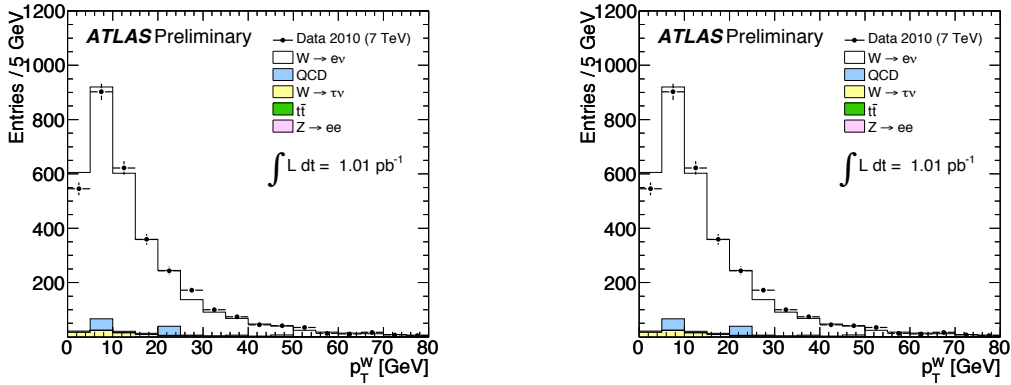

Figure 3: p_T of the W candidates in the electron-channel (left) and muon-channel (right) after final selection. The integrated luminosity is $\approx$ 1 pb^{-1}, corresponding to a larger data set than the one used for the measurement.
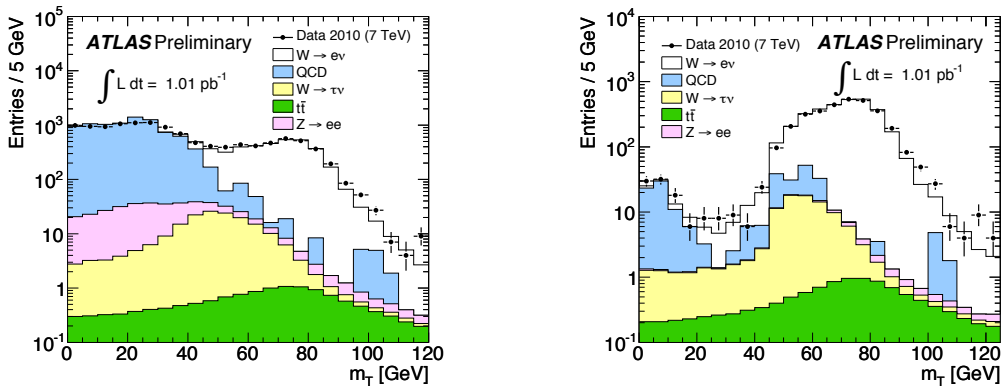

Figure 4: $M_T(W)$ of the electron-E_T system without (left) and with (right) a requirement of $E_T > 25$ GeV. The integrated luminosity is $\approx$ 1 pb^{-1}, corresponding to a larger data set than the one used for the measurement.

5.1.2 Background estimation

The remainder of QCD background after all cuts is estimated directly from data, given the scarce knowledge of the production of secondary leptons from the QCD processes used in the simulation. More specifically, two different approaches are used in the electron and muon channels. For the latter,the QCD processes generating electrons are HF decays and hadrons identified as electrons, on top of QED processes like photon conversions into an e^+e^- pair. To estimate the QCD contribution in the selected sample, we rely on the distribution of the calorimeter isolation, defined as the sum of energy deposited in the cells of the e.m. and hadronic calorimetry within a cone of $\Delta R = 0.4$ around the electron momentum. To measure the amount of QCD decays selected we release the electron definition in order to enhance the background contribution; and we look at the distribution of the isolation for *Loose* electrons. Given the higher statistics of the looser electron sample, we fit the isolation distribution in data with Monte Carlo templates and then extrapolate the simulated isolation into the signal region for *Loose* electrons passing all other analysis cuts. The isolation for the initial and final samples of *Loose* electrons are shown in Figure 5. By doing so,
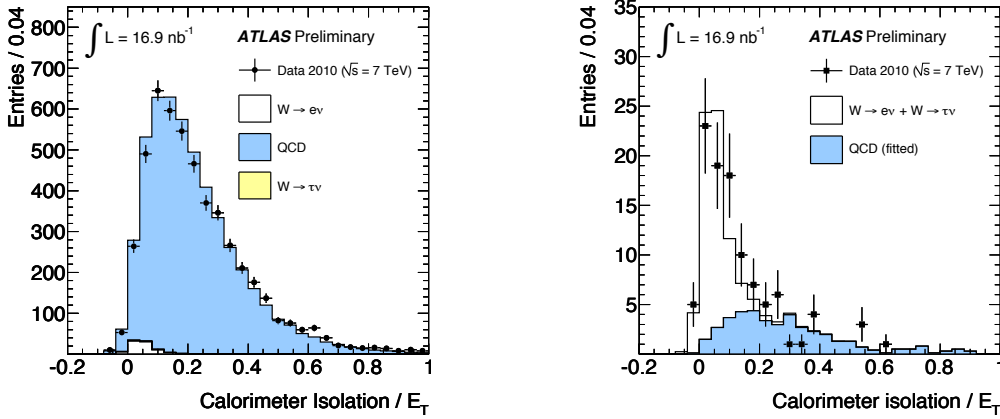

Figure 5: Left: Calorimeter isolation variable divided by E_T after preselection. Right: result of the template fit where the event selection contains all requirements but that of being a *Tight* electron (these are *Loose* electrons)

we estimate the amount of contributing QCD events to be: 1.1 ± 0.2 (stat) ± 0.4 (syst). For the muon channel, we predict the background rate in the signal region from control regions dominated by backgrounds (HF and π and K decays into muons). In particular, considering two *uncorrelated* variables on which signal selections are applied (in our case E_T^{miss} and the track-based isolation relative to the muon p_T), one can extrapolate the level pf QCD contribution in the three control areas ouside the signal region into the latter, enriched in $W \rightarrow \mu\nu$ signal. This is illustrated in Figure 6, and the estimated number of QCD events in the signal region is : 0.9 ± 0.3 (stat) ± 0.6 (syst).

5.1.3 Event yields and acceptance corrections

Table 1 [11] summarizes the expected amount of signal, electroweak and QCD backgrounds selected, where the electroweak one is extracted from simulation, since we have a better knowledge of the electroweak production processes than the QCD ones.
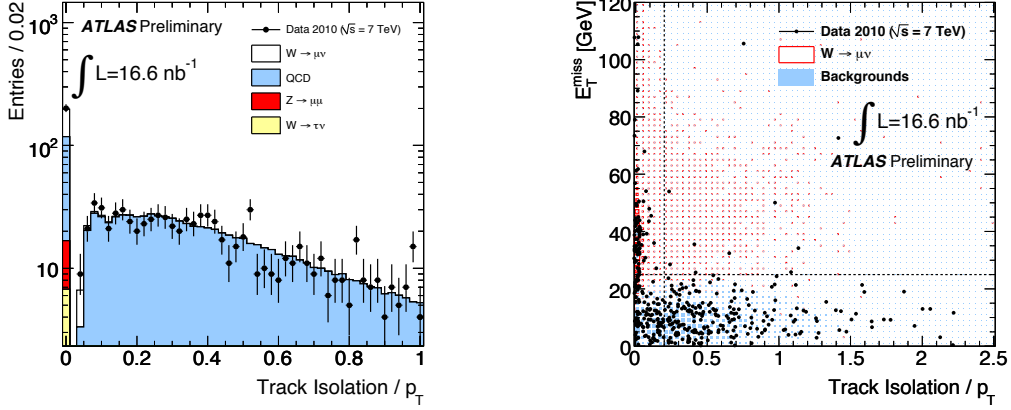
Figure 6: Left: Track-isolation variable $\Sigma p_T(ID)/p_T$. Right: E_T^{miss} vs $\Sigma p_T(ID)/p_T$ for muon candidates. In both cases the integrated luminosity is 16.6 nb^{-1}.

ℓ	Observed candidates	Background (EW)	Background (QCD)	Background-subtracted signal N_W^{sig}
e^+	27	$0.9 \pm 0.0 \pm 0.1$	$0.6 \pm 0.1 \pm 0.3$	$25.6 \pm 5.2 \pm 0.3$
e^-	19	$0.6 \pm 0.0 \pm 0.1$	$0.6 \pm 0.1 \pm 0.3$	$17.8 \pm 4.4 \pm 0.3$
$e^\pm$	46	$1.5 \pm 0.0 \pm 0.1$	$1.1 \pm 0.2 \pm 0.4$	$43.4 \pm 6.8 \pm 0.4$
μ^+	47	$2.4 \pm 0.0 \pm 0.2$	$0.7 \pm 0.3 \pm 0.5$	$43.8 \pm 6.9 \pm 0.6$
μ^-	25	$2.0 \pm 0.0 \pm 0.2$	$0.2 \pm 0.1 \pm 0.2$	$22.8 \pm 5.0 \pm 0.3$
$\mu^\pm$	72	$4.4 \pm 0.0 \pm 0.3$	$0.9 \pm 0.3 \pm 0.6$	$66.7 \pm 8.5 \pm 0.7$

Table 1: Numbers of observed candidate events for the $W \to \ell\nu$ channel, electroweak (EW) and data-derived QCD background events, and background-subtracted signal events, from [11]. The first uncertainty is statistical (Monte Carlo statistical errors are negligible). The second uncertainty represents the systematics. In addition to what is quoted in this table, an 11% uncertainty on the luminosity determination is applicable to the electroweak background.

In order to extract the production cross-section from these event yields, we need to fold in the information on the acceptance, estimated from simulation, following the formula:

$$\sigma_{tot} = \sigma_W \times BR(W \to \ell\nu) = \frac{N_W^{sig}}{A_W C_W L_{int}}, \tag{5.2}$$

where

- N_W^{sig} denotes the number of background-subtracted signal events in the channel of interest, as summarised in Table 1;

- A_W represents the geometrical acceptance for the given channel, defined as the fraction of decays satisfying the geometrical and kinematical (fiducial) constraints at the generator level (lepton kinematic requirements, missing transverse energy cut and $M_T(W) > 40$ GeV at the

generator level). This quantity can only be determined from $W \rightarrow \ell \nu$ Monte Carlo simulation at generator level;

- C_W is the ratio between number of signal events which pass the final selection requirements after reconstruction and the total number of generated events within the fiducial volume (efficiency for triggering on lepton candidates as well as reconstructing/identifying the W boson decays falling within the geometrical acceptance). C_W is fully determined from simulation for the electron channel, while data-driven corrections for the trigger efficiency and the efficiency to reconstruct and identify a muon are used for the muon channel;

- finally L_{int} denotes the integrated luminosity for the channel of interest.

Values from simulation for the trigger and identification efficiency for the electron channel are (0.999 ± 0.001) and (0.78 ± 0.05). For the muon channel the corresponding values are $(0.88 \pm 0.01(stat) \pm 0.03(syst))$ and $(0.97 \pm 0.01(stat) \pm 0.04(syst))$ respectively. The difference in the trigger efficiency rises from geometrical acceptance, due to the reduced coverage of the muon trigger chambers close to the toroid coils; on the contrary, the muon reconstruction efficiency is higher than then one of the electrons, due to the tight selections aimed at reducing the large backgrounds in the electron identification. Scale factors to match simulation expectations with data are also measured for the muon analysis, and their values are: $(0.97 \pm 0.01(stat) \pm 0.04(syst))$ and $(0.99 \pm 0.01(stat) \pm 0.04(syst))$ for trigger and identification respectively.

5.2 Measured cross sections

Given the yields and acceptance terms summarised before it is possible to proceed to measure the production cross sections for W^+, W^- and $W^\pm$. The total cross sections are presented in Table 2, together with their statistical, systematic and luminosity uncertainties. The total cross section values for the combined electron-muon channels, when taking into account the correlated and uncorrelated sources of uncertainty, are $\sigma_{tot}(W^+) = [5.7 \pm 0.7(\text{stat}) \pm 0.4(\text{syst}) \pm 0.6(\text{lumi})]$ nb, $\sigma_{tot}(W^-) = [3.5 \pm 0.5(\text{stat}) \pm 0.2(\text{syst}) \pm 0.4(\text{lumi})]$ nb, and $\sigma_{tot}(W^\pm) = [9.3 \pm 0.9(\text{stat}) \pm 0.6(\text{syst}) \pm 1.0(\text{lumi})]$ nb. The expected theoretical calculation of the cross-section at Next-to-Next-to-Leading-Order (NNLO) QCD corrections is performed using the FEWZ [12] program using the MSTW2008 NNLO structure function parameterisation [13]. The renormalisation scale μ_R and factorisation scale μ_F were chosen to be $\mu_F = \mu_R = m_W$. Figure 7 (where the electron and muon channels are shown separately) shows that, within the experimental uncertainties, the measured cross sections agree well with the calculations for both W^+ and W^- production and the expected asymmetry between these cross sections is confirmed experimentally. No theoretical uncertainties resulting from variations of the renormalisation and factorisation scales as well as uncertainties resulting from structure-function parameterisations are shown (order of $\pm 4\%$ at 7 TeV).

5.3 Z boson analysis

Similar to the W boson case, we perform an event selection based on good-quality leptons in the final state, evaluate the yields for signal and backgrounds and the selection acceptances; and proceed to measure for the first time in ATLAS the production cross-section of the Z boson.

		W^+				W^-				$W^\pm$		
		Electron channel										
	value	stat	syst	lumi	value	stat	syst	lumi	value	stat	syst	lumi
Background- subtracted signal	25.6	5.2	0.3	0.1	17.8	4.4	0.3	0.1	43.4	6.8	0.4	0.2
Correction C_W	0.653	-	0.052	-	0.660	-	0.053	-	0.656	-	0.053	-
Acceptance A_W	0.466	-	0.014	-	0.457	-	0.014	-	0.462	-	0.014	-
Total cross section (nb)	**5.0**	**1.0**	**0.4**	**0.5**	**3.5**	**0.9**	**0.3**	**0.4**	**8.5**	**1.3**	**0.7**	**0.9**
		Muon channel										
	value	stat	syst	lumi	value	stat	syst	lumi	value	stat	syst	lumi
Background- subtracted signal	43.8	6.9	0.6	0.3	22.8	5.0	0.3	0.2	66.7	8.5	0.7	0.5
Correction C_W	0.822	-	0.057	-	0.804	-	0.057	-	0.814	-	0.056	-
Acceptance A_W	0.484	-	0.014	-	0.475	-	0.014	-	0.480	-	0.014	-
Total cross section (nb)	**6.6**	**1.0**	**0.5**	**0.7**	**3.6**	**0.8**	**0.3**	**0.4**	**10.3**	**1.3**	**0.8**	**1.1**

Table 2: Results for the total cross section σ_{tot} for W^+, W^-, and $W^\pm$ in the electron and muon channels. Shown are the observed numbers of signal events after background subtraction for each channel, the average correction factors C_W, the fiducial cross sections, the geometrical acceptance correction factors, and the total cross sections with their statistical, systematic, and luminosity uncertainties quoted in that order.
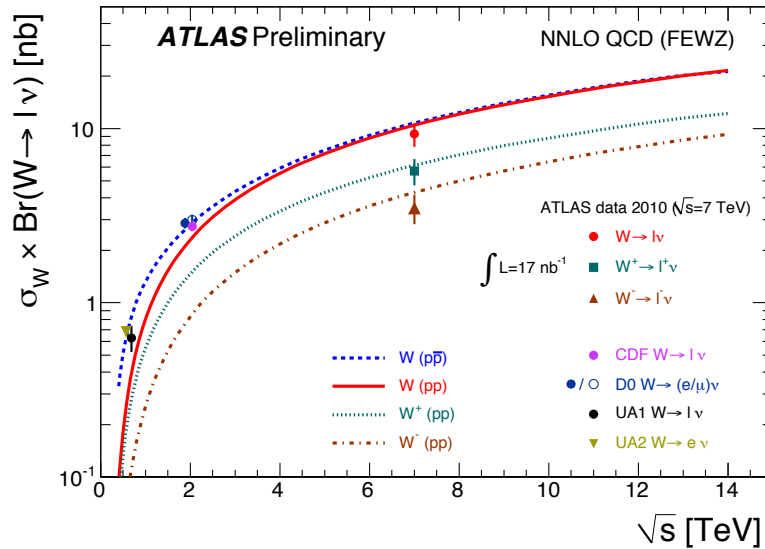

Figure 7: The measured values of $\sigma_W \times BR(W \to \ell\nu)$ compared to the theoretical predictions based on NNLO QCD calculations. Results are shown for the combined electron-muon channels, for an integrated luminosity of 17 nb^{-1}

In this case, the following selections are applied at the lepton and event level, for the electron channel:

- the event is selected by the ATLAS Level-1 trigger requiring $|\eta(\text{calorimetric object})| < 2.5$ and $E_T > 10$ GeV;

- exactly two *Medium* electrons reconstructed offline, with an energy in the transverse plane $E_T > 20$ GeV and opposite electric charge;

The following selections are applied for the muon channel:

- the event is selected by the ATLAS Level-1 trigger requiring $|\eta(\text{muon object})| < 2.4$ and $E_T > 6$ GeV;

- exactly two combined muons reconstructed offline, with a momentum in the transverse plane $p_T > 20$ GeV and opposite electric charge;

- the sum of the p_T of ID tracks closer than $\Delta R = 0.4$ to each muon, normalized to the muon p_T should be less than 0.2, as an isolation criterion;

The invariant mass of the selected lepton pairs is shown in Figure 8 for both lepton types, and a fit to the distibution is overlaid to estimate the actual width and the difference with respect to the expectations from Monte Carlo simulation. The fit is performed using the theoretical Z boson lineshape convoluted with a Gaussian function to model the detector resolution. For the electrons, the fitted width on data is (3.2 ± 0.3) GeV, compatible with expectations from test beam and the *in-situ* calibration of the e.m. calorimetry with $\pi^0 \rightarrow \gamma\gamma$ decays; for the muons the width is (3.3 ± 0.3) GeV and it is larger than expectations due to the initial misalignment of the ID and MS. 46 (79) events are selected and fall within the $66 < M(\ell\ell) < 116$ GeV range for the electron (muon)
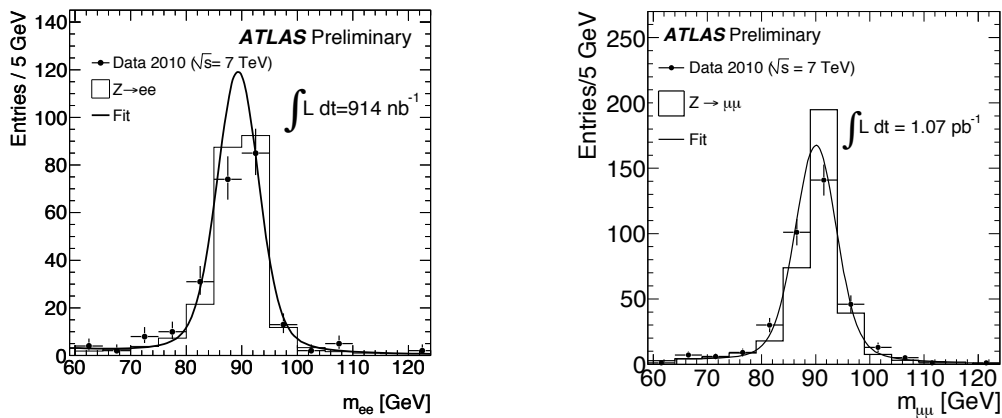

Figure 8: Invariant mass $M_{\ell\ell}$ of Z boson candidates in the electron (left) and muon (right) channels, overlaid with simulation and a fit to data. The integrated luminosity is ≈ 1 pb^{-1}, corresponding to a larger data set than the one used for the measurement.

channel, for 219 (229) nb^{-1} of integrated luminosity. For this analysis the backgrounds are fully estimated from MC. In particular, for the electron channel results on MC for the *Loose* category

	Z							
	Electron channel				**Muon channel**			
	value	stat	syst	lumi	value	stat	syst	lumi
Background-subtracted signal	45.5	6.8	-	-	78.8	8.9	-	-
Correction C_Z	0.645	-	0.090	-	0.797	0.013	0.053	-
Acceptance A_Z	0.446	-	0.013	-	0.486	-	0.014	-
Total cross section (nb)	**0.72**	**0.11**	**0.10**	**0.08**	**0.89**	**0.10**	**0.07**	**0.10**

Table 3: Results for the fiducial cross sections σ_{fid} and total cross section σ_{tot} for Z boson in the electron and muon channels. Shown are the observed numbers of signal events after background subtraction for each channel, the average correction factors C_Z, the fiducial cross sections, the geometrical acceptance correction factors, and the total cross sections with their statistical, systematic, and luminosity uncertainties quoted in that order.

(higher statistics) are extrapolated into the Medium category, predicting a rate of QCD events in the signal region of 0.49 ± 0.07 (stat) ± 0.05 (syst), which compares well with the rate of electron pairs with *same* electric charge, equal to 1. For the muon channel, expectations from Monte Carlo in the signal region are: 0.17 ± 0.01 (stat) ± 0.01 (syst), with no muon pairs of same electric charge passing all cuts.

The correction factors to the cross-section due to the acceptance at the generator and reconstruction level are estimated, also in this case, from simulation; and uncertainties on the A_Z and C_Z parameters depend on Leading-Order versus Next-to-Leading-Order differences and trigger and reconstruction data/simulation discrepancies, respectively.

The derived Z boson production cross sections for both the electron and muon channels within the invariant mass window $66 < m_{ee} < 116\,\mathrm{GeV}$ are presented in Table 3, along with their statistical, systematic, and luminosity uncertainties. The total cross section value for the combined electron-muon channels, when taking into account the correlated and uncorrelated sources of uncertainty, is $\sigma_{tot} = [0.83 \pm 0.07(\mathrm{stat}) \pm 0.06(\mathrm{syst}) \pm 0.09(\mathrm{lumi})]$ nb

The comparison with the theoretical calculations at NNLO and previous experiments at $p\bar{p}$ colliders is displayed in Figure 9 and shows a good description of the Z boson production cross-section with energy.

6. W and Z boson production in association with jets

With 1 pb^{-1} of integrated luminosity from LHC collision data available at the time of this presentation it is also possible to start probing the agreement of data and simulation in terms of additional activity present in the detector along with an electroweak object. The W and Z cross-section differential measurement in jet multiplicity, infact, is not only an important benchmark number per se to probe our theoretical understanding of initial and final state radiation mechanism in hadronic interactions, but experimentally it is also relevant as $W + n$ jets and $Z + n$ jets are important backgrounds in all *high-p_T* physics, from top quark measurements to searches for new physics processes like supersymmetric ones. While the measurements described in the previous
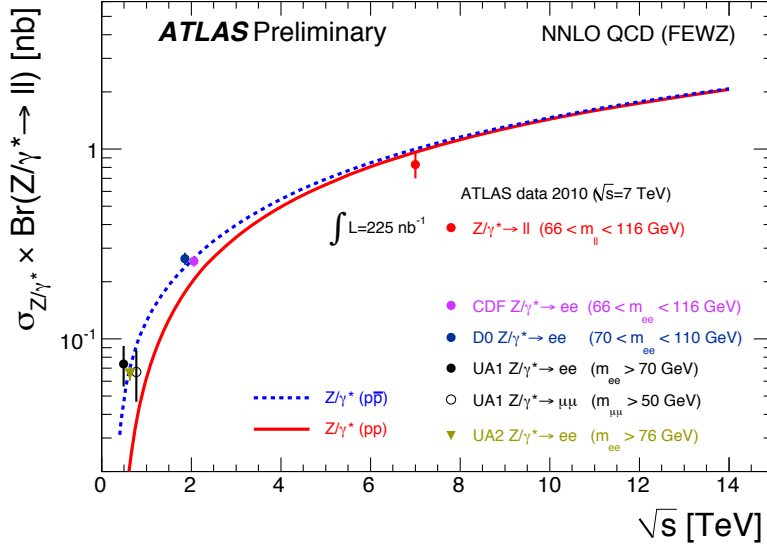
Figure 9: The measured values of $\sigma_Z \times BR(Z \to \ell\ell)$ compared to the theoretical predictions based on NNLO QCD calculations.

sections are completely inclusive in that respect, and only look at the *W* and *Z* boson decays, some initial comparisons in this direction are performed. In this presentation we showed preliminary results based on 0.9 pb^{-1}, in which the agreement between data and Monte Carlo simulation is checked in terms of jet multiplicity and p_T of the highest-p_T jet in the *W* or *Z* selected event. Jets are reconstructed using the anti-k_T jet algorithm [14], with R=0.4. Also, their absolute pseudorapidity should be within 2.8, and $p_T > 20$ GeV. The results are shown for the *W* and *Z* bosons separately, but for the electron and muon channel together, in Figures 10 and 11, and they show already a remarkable agreement in shape and kinematic distribution between data and simulation. At this stage the background shapes (mainly QCD processes and, at high multiplicity and high p_T also $t\bar{t}$ decays) are estimated from simulation, while the normalization is scaled according to the scale factors from the inclusive analysis.

7. First $t\bar{t}$ candidates

The $W + n$ jets and $Z + n$ jets are an important background for any measurement involving a pair of top quarks. In this initial phase of the LHC and ATLAS detector running we search for $t\bar{t}$ pair production, using final states with one or two leptons. $t\bar{t}$ are infact a primary testing ground before endeavouring in any new physics searches in the *high-p_T* region, as they show up with leptons, transverse missing energy due to the neutrinos from the *W* boson decay, and a large number (typically 4 for the semileptonic channel) additional jets. Therefore, they test all our ability to reconstruct neighbouring physics objects.

To search for semileptonic (dileptonic) $t\bar{t}$ candidates we require that an event pass the following selections:

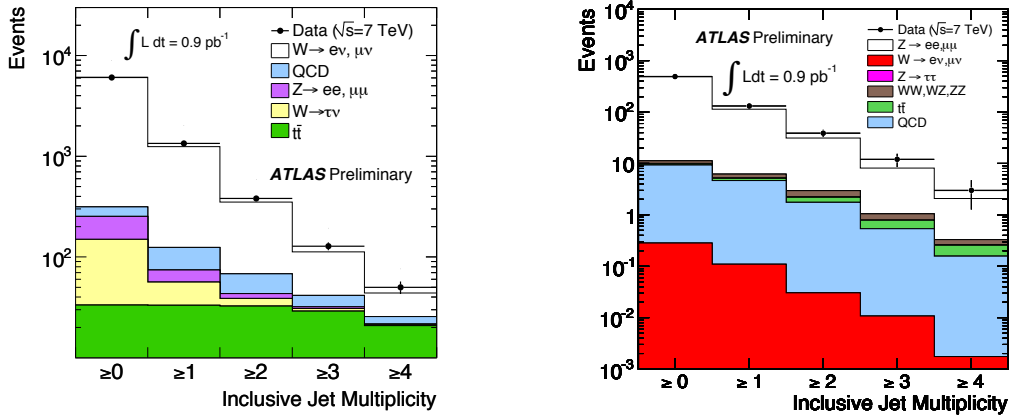- 10 GeV single lepton trigger at Level-1;

13

Figure 10: Multiplicity of anti-k_T R=0.4 jets accompanying a *W* (left) and *Z* (right) boson candidate, combining electron and muon channels. The Monte Carlo is normalized to the inclusive data sample.
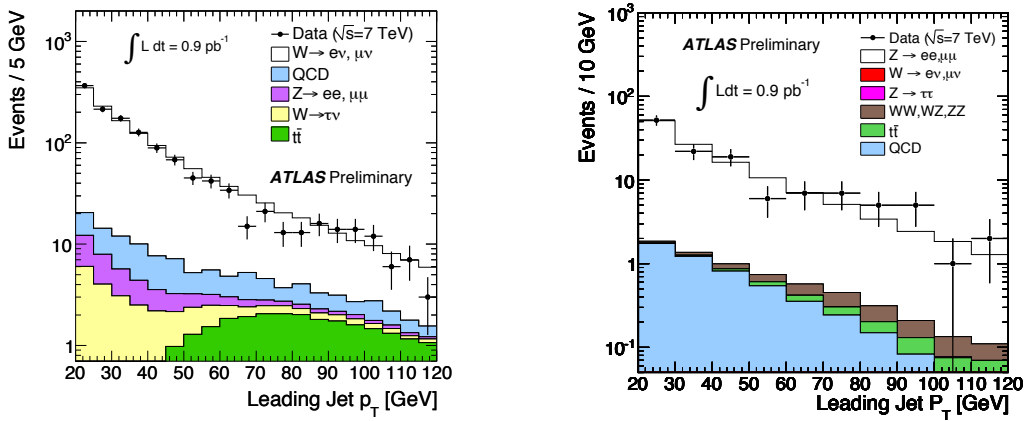

Figure 11: p_T of the leading anti-k_T R=0.4 jet accompanying a *W* (left) and *Z* (right) boson candidate, combining electron and muon channels. The Monte Carlo is normalized to the inclusive data sample.

- exactly one (two) lepton (*Medium e* or *Combined* μ) having $p_T > 20$ GeV and $|\eta| < 2.5$;

- the leptons should also be isolated in the calorimeter and, for the muon, also in the ID;

- at least 4 (2) jets reconstructed by the anti-k_T algorithm with R=0.4, and a $p_T > 20$ GeV;

- for the semileptonic channel: 1 jet identified as a jet from a *b* quark decay, with a tagging figureof-merit corresponding to a 50% *b*-jet efficiency;

- $E_T^{miss} > 20$ GeV (semileptonic), 30 GeV (*ee*) and 40 GeV ($\mu\mu$);

Since the full kinematic information is not available experimentally in the dileptonic channel due to the neutrinos, we cannot reconstruct the top quark mass as in the semi-leptonic case. Additional requirements are applied to reject the backgrounds in the dileptonic channel:

- *Z* boson mass veto for the two, opposite-charge, leptons;

- $\Sigma p_T(lep, jet) > 150$ GeV for the ($e\mu$ channel);

7 (2) candidates are identified in 280 nb^{-1} for the semi-leptonic (di-leptonic) channel. The distribution of the reconstructed masses of the hadronically decaying top quarks is shown in Figure 12 for the electron and muon channels. The main backgrounds for the single lepton channel are the
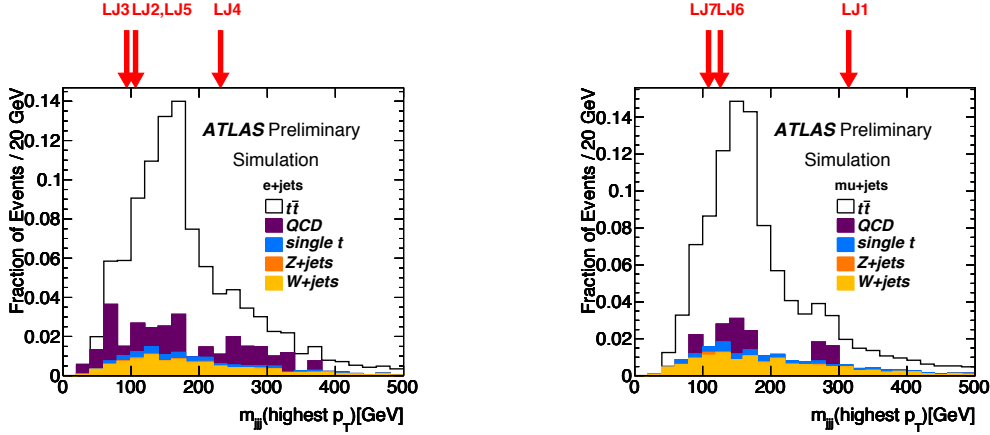

Figure 12: Left: Distribution of the invariant mass of the 3-jet combination having the highest p_T, for events passing the electron plus jets (left) and muon plus jets (right) selections.

QCD processes in which one lepton is produced by a HF decay (which is being measured directly in data using the so-called *Matrix method* [15]) and $W + n$ jets processes, estimated at the stage of the presentation only from simulation.

8. Conclusions

In summary, we have reviewed the initial results on the electroweak physics with the ATLAS detector using different integrated luminosities (from 17 nb^{-1} to 0.9 pb^{-1}) from pp interactions at the LHC. The measurements of the inclusive W and Z boson cross-sections gave in particular both a chance to test the Standard Model expectations on W and Z boson production scaling with the centre-of-mass energy; and to commission the ATLAS detector with early data. With more data, an accurate measurement of the expected W charge asymmetry; exclusive measurements of $W + n$ and $Z + n$ jet cross-sections; and a measurement of the $t\bar{t}$ cross-section relying on data to estimate electroweak and QCD backgrounds are envisaged.

9. Acknowledgments

References

[1] K. Nakamura et al. (Particle Data Group), *Review of Particle Properties*, J. Phys. G 37, 075021 (2010)

[2] The ATLAS Collaboration, G. Aad *et al*, *The ATLAS Experiment at the CERN Large Hadron Collider*, JINST 3 (2008) S08003

[3] T. Sjostrand, S. Mrenna, and P. Skands, *PYTHIA 6.4 physics and manual*, JHEP 05 (2006) 026

[4] A. Sherstnev and R. S. Thorne, *Parton Distributions for LO Generators*, Eur. Phys. J. C55 (2008) 553

[5] S. Frixione and B.R. Webber, *Matching NLO QCD computations and parton shower simulations*, JHEP 06 (2002) 029, arXiv:hep-ph/0204244; S. Frixione, P. Nason and B.R. Webber, *Matching NLO QCD and parton showers in heavy flavour production*, JHEP 08 (2003) 007, arXiv:hep-ph/0305252; S. Frixione, E. Laenen and P. Motylinski, *Single-top production in MC@NLO*, JHEP 03 (2006) 092, arXiv:hep-ph/0512250

[6] P.M. Nadolsky et al., *Implications of CTEQ global analysis for collider observables*, Phys. Rev. D78 (2008) 013004, arXiv:0802.0007 [hep-ph]

[7] S. Moch and P. Uwer, *Theoretical status and prospects for top-quark pair production at hadron colliders*, Phys. Rev. D78 (2008) 034003, arXiv:0804.1476 [hep-ph]; U. Langenfeld, S. Moch, and P. Uwer, *New results for $t\bar{t}$ production at hadron colliders*, arXiv:0907.2527 [hep-ph]

[8] The ATLAS Collaboration, G. Aad *et al*, *Search for top pair candidate events in ATLAS at $\sqrt{s} = 7$ TeV*, `https://atlas.web.cern.ch/Atlas/GROUPS/PHYSICS/CONFNOTES/ATLAS-CONF-2010-063/`

[9] The GEANT4 Collaboration, S. Agostinelli et al., *GEANT4: A simulation toolkit*, Nucl. Instrum. Meth. A506 (2003) 250

[10] The ATLAS Collaboration, G. Aad *et al*, *Measurement of the $W \to \ell\nu$ and $Z/\gamma^* \to \ell\ell$ production cross sections in proton-proton collisions at $\sqrt{s} = 7$ TeV with the ATLAS detector*, arXiv:1010.2130 [hep-ex] (submitted to JHEP)

[11] The ATLAS Collaboration, G. Aad *et al*, *Measurement of the $W \to \ell\nu$ production cross-section and observation of $Z \to \ell\ell$ production in proton-proton collisions at $\sqrt{s} = 7$ TeV with the ATLAS detector*, `https://atlas.web.cern.ch/Atlas/GROUPS/PHYSICS/CONFNOTES/ATLAS-CONF-2010-051/`

[12] C. Anastasiou, L. Dixon, K. Melnikov, and F. Petriello, *High-precision QCD at hadron colliders: electroweak gauge boson rapidity distributions at NNLO*, Phys. Rev. D69 (2004) 094008

[13] A. D. Martin, W. J. Stirling, R. S. Thorne, and G. Watt, *Parton distributions for the LHC*, Eur. Phys. J. C63 (2009) 189285

[14] M. Cacciari, G. Salam, and G. Soyez, *The anti-k_T jet clustering algorithm*, JHEP 0804 (2008) 063, arXiv:0802.1189

[15] The ATLAS Collaboration, G. Aad *et al*, *Background studies for top-pair production in lepton plus jets final states in $\sqrt{s} = 7$ TeV ATLAS data*, `https://atlas.web.cern.ch/Atlas/GROUPS/PHYSICS/CONFNOTES/ATLAS-CONF-2010-087/`